A&A 388, 540–545 (2002)
DOI: 10.1051/0004-6361:20020572

Astronomy & Astrophysics

Wavelet analysis of stellar differential rotation

II. The Sun in ultraviolet

A. Hempelmann⋆

Universität Hamburg, Hamburger Sternwarte, Gojenbergsweg 112, 21029 Hamburg, Germany

Received 17 December 2001 / Accepted 11 April 2002

Abstract. Among the several methods to study differential rotation on stellar surfaces the observation of a stellar butterfly diagram, i.e. monitoring the rotation period over a complete activity cycle, is the only method which can be applied to stars rotating as slow as the Sun. However, the method requires active belts on the stellar surface which are moving continously in stellar latitude during a cycle. In addition, an appropriate activity tracer showing rotational modulation is needed. Tracers which even work for slowly rotating, i.e. weakly active, stars are the emission cores of certain spectral lines. However, the question is whether surface differential rotation can be determined from this kind of observations and furthermore, which method of analysis is best suited to yield a correct result. We investigate observations of the Sun as a star, i.e. disk-integrated measurements, to answer these questions. In a Paper I it was demonstrated that time-frequency analysis using the wavelet transform is possibly a suitable method for monitoring the stellar butterfly diagram. It was also shown that – in comparison with Fourier analysis – wavelet analysis of disk-integrated solar Ca II K line core emission measures yield a much more realistic pattern of the solar differential rotation. In this Paper II disk-integrated solar measures in Mg II h+k and Lyman α taken from public UARLS Solstice data are analysed using the same methods as in Paper I. In these data solar rotational modulation is much more pronounced than in earlier Ca II K time-series. Wavelet analysis yields the following results: from the beginning of the time-series in 1991 until the end of solar cycle 22 the period of rotational modulation remains stable at 26.9–27.0 days. It is followed by a jump to 27.6 days when the new cycle 23 starts. Then the period rapidly decreases to 26.9 days again until the end of the time-series in 1999. However, the analysis is hampered by frequent period splitting into two modes. It can be shown that this kind of splitting results from phase jumps in the time-series coming from active region growth and decay at 180° shifted solar longitudes.

Key words. Sun: rotation – stars: rotation – methods: data analysis

1. Introduction

Differential rotation is a key parameter for the solar and stellar dynamo, its observation is an important task. While differential rotation of the Sun can be modelled by theory (Kitchatinov & Rüdiger 1995; Kitchatinov & Rüdiger 1999) the task remains somewhat open for stars others than the Sun.

Available methods for the study of surface differential rotation on stars are:
i) investigating rotational broadening of stellar spectral lines, i.e. line profile analysis;
ii) monitoring of star spots by Doppler tomography;
iii) constructing stellar butterfly diagrams by monitoring the period of rotational modulation of certain activity tracers over a complete activity cycle.
While the first two methods are limited to fast rotators with rotation periods typically ranging from hours to a few days, application of the third method is basically independent of the stellar rotation period. The only requirements are that active regions are inhomogenously distributed over the stellar surface to cause rotational modulation of an activity tracer and that their mean latitude varies during an activity cycle. Both conditions are obviously satisfied for the Sun. They are reasonable to assume for other stars, too, if a similar dynamo mechanism is at work there.

Tracers which show a measurable rotational modulation are the emission cores of certain spectral lines. The most important lines are CaII H+K in the optical spectral range and MgII h+k in the ultraviolet. Stellar butterfly diagrams were observed using CaII H+K data from Mount Wilson Observatory's HK Project (Baliunas et al. 1985; Donahue et al. 1996; Gray & Baliunas 1997). These observations showed solar-type differential rotation as well as strong deviations from the solar behaviour. Frequently

⋆ e-mail: ahempelmann@hs.uni-hamburg.de

two periods of rotational modulation were detected; an extreme example for such behaviour is β Com (Gray & Baliunas 1997). The question is: are there really two different kinds of rotation patterns on stellar surfaces or is it an artefact caused by intrinsic variability of the activity tracer? Such an intrinsic variability could be caused by active region growth and decay.

The Sun may turn out to be a kind of Rosetta stone. The solar surface pattern of differential rotation is known and can be compared with the result from observations of the Sun observed as a star, i.e., from measures integrated over the solar disk. Donahue & Keil (1995) analysed solar disk-integrated CaII K data and found the correct qualitative behaviour: a jump from short rotation period at the end of an activity cycle to long rotation period at the beginning of a new cycle. However, using Fourier analysis, the amplitude of differential rotation they found was much too high. Applying wavelet analysis to nearly the same data Hempelmann & Donahue (1997, Paper I) found a significant smaller amplitude. However, comparing their result to solar observations in detail (cf., Fig. 10 in the paper by Gray & Baliunas 1997) the amplitude they found still seems to be a bit too large. In this Paper II, I continue this investigation by help of two other chromospheric activity tracers: MgII h+k and Lyman α.

2. Observations

In this paper, daily observations from the Solar Stellar Irradiance Comparison Experiment (SOLSTICE) on board of the NASA's Upper Atmosphere Research Satellite (UARS) are investigated. The Sun has been observed as a star since 1991 by this instrument. The observations are done disk-integrated without spatial resolution of details of the solar surface resp. throughout the solar atmosphere. Therefore an investigation of Solstice data should be a powerful tool to test methods applied to stars.

The instrument is based on a spectrometer covering the spectral range between 115 and 430 nm with a spectral resolution of 0.1–0.3 nm. It was designed to study the solar ultraviolet energy output (Rottman et al. 1993). The measurements are calibrated using 30 non-variable O-B-A stars which are regularily observed during portions of the spacecraft orbit when the instrument does not observe the Sun (Woods et al. 1993). From these raw data several time series in form of daily means were generated and published in the Internet, among them a MgII k line index and a Lyman α irradiance measure (Knapp 2000).

The MgII h+k measure is a flux ratio of the integrated intensity of the k emission line core to an averaged continuum in the line wings. Each integration interval is 0.125 nm broad. While this Mg S index is a relative flux the Lyman α measure is an absolute flux derived by integrating over the whole line profile and subtracting the continuum.

Measurements and data reduction are described in detail by Knapp (2000). A validation of both measurents were performed by Woods et al. (1996).

The UARS Solstice spectrometer provides time-series in which both the solar activity cycle and the solar (synodic) rotation period can be detected (Chandra et al. 1995). The latter type of variability shows strong modulation of the amplitude with the phase of the activity cycle. At activity maximum the observed amplitude is larger than at solar activity minimum (Rottman 1999). The amplitude of the rotational modulation also depends on the wavelength: the shorter the wavelength in UV the higher the amplitude. An exception is MgII h+k where amplitudes almost as high as in Lyman α are observed (Rottman 1999). Hence MgII h+k as well as Lyman α seem to be most promising to study the solar rotation in more detail. In the next chapter the correlation between the observed period of rotational modulation and the phase of the activity cycle is investigated to answer the question whether both MgII h+k and Lyman α are appropriate activity indicators to study surface differential rotation on stars.

3. Correlation of rotation period with cycle phase

3.1. Data analysis

The method of data analysis has been described in Paper I. It is based on Fourier analysis as well as on wavelet analysis. Figures 1 and 2 show the two time-series between 1991 and 1999. Both time-series show almost identical structure. The solar activity cycle ranging from maximum to minimum of solar cyle 22 into rising activity of the beginning cycle 23 is clearly present. On shorter time-scales rotational modulation dominates. Variability on medium time-scales is also present. This may be caused by active region growth and decay (ARGD). Skumanich et al. (1984) and Worden et al. (1998) have shown that both plage and active network areas are the main sources of chromospheric variability. The life-time of a plage is 1–3 solar rotations (Foukal 1998) whereas the process of an active network turning into a quiet network may last for several rotations. Woods et al. (2000) determined the typical time scale of this process as nine solar rotations.

Long-term and medium-term variability were removed by fitting low-order splines and setting the mean values to zero. Finally the (few) gaps in the data were filled in with zero. The resulting data (cf., Fig. 3) serve as a basis of the following analysis.

In a first step Fourier analysis was done. Figures 6 and 7 show Fourier power spectra extracted from these reduced time-series. The spectrum is dominated by a series of peaks in the range between 26 and 28 days, i.e., solar rotation. The dominant peak appears at 27.2 days which is a typical mean value of solar synodic rotation (Cox 2000). Minor peaks appear at the first harmonics and in the range of 80–200 days. I suppose the latter is the consequence of amplitude modulation of the 27 days

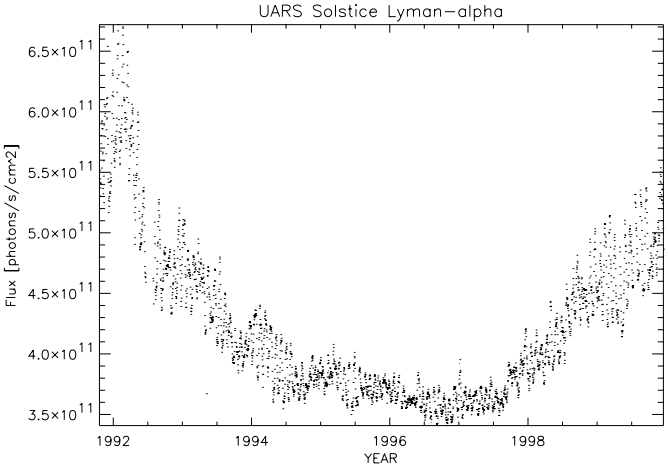

Fig. 1. Time-series of UARS Solstice Lyman-α fluxes.

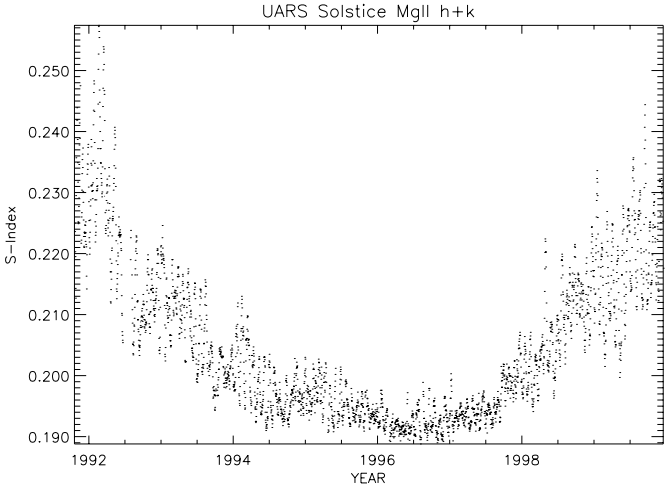

Fig. 2. Time-series of UARS Solstice MgII h+k core to wing flux ratios.

period caused by ARGD. Figure 3 shows a general trend of increasing amplitude with increasing activity superimposed by strong fluctuations on medium time-scales between the solar cycle and rotation.

The appearence of isolated peaks in the 27 days range is somewhat surprising. A continous variation would be expected in case of a continous shift of the observed rotation period over the activity cycle. To study the temporal behaviour of the rotation period observed, a time-frequency analysis is required. As explained in Paper I wavelet analysis was chosen.

The spectral and time resolution parameter a was chosen as the same value as in Paper I: $a = 0.005$ giving a resolution of 0.5 days in the rotation period and a time resolution of 300 days.

3.2. Expected artefacts

The resolutions in time and frequency (or period) are inversely correlated. Hence, the art of time-frequency analysis is finding an optimum balance in the resolutions. However, resolution will be limited and this has to be

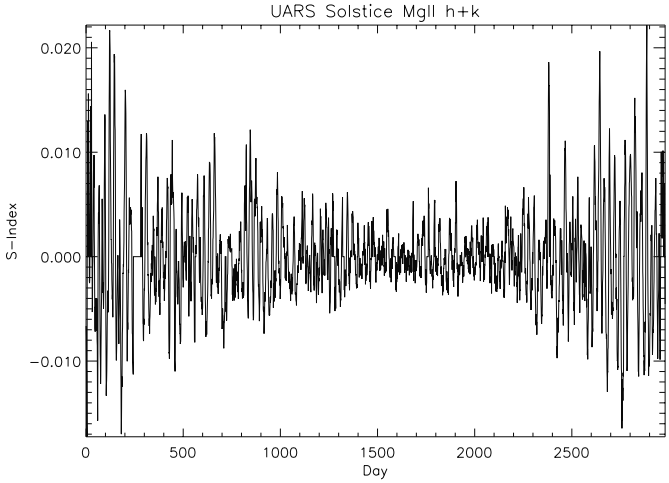

Fig. 3. Reduced time-series.

taken into account when interpreting the wavelet map (or any other result yielded by time-frequency analysis). Another important effect which has to be taken into account is frequency shift as the consequence of a variable phase element of an oscillation. (I am deeply indepted to the (anonymous) referee who pointed this out to me.) This can be caused either by a variable period or by a variable zero phase. (The latter will be investigated in the next chapter.) Both effects play an important role for the interpretation of stellar butterfly diagrams. Even a slow change of the rotation period as a consequence of differential rotation can cause a remarkably large shift between the intrinsic and the observed period. Let $P_\mathrm{o} + \alpha t$ the intrinsic period which shall vary linearily with time. Then the observed frequency

$$\frac{\mathrm{d}\phi}{\mathrm{d}t} = \frac{\mathrm{d}(\frac{t}{P_\mathrm{o}+\alpha t})}{\mathrm{d}t} = [(P_\mathrm{o} + \alpha t)(\frac{P_\mathrm{o} + \alpha t}{P_\mathrm{o}})]^{-1} \quad (1)$$

contains a factor which causes a shift between the intrinsic period and the observed period. Simulating a solar-like case with cycle 11 years and period variation of one day over the cycle one gets $\alpha = 0.00025$. In Fig. 4 the wavelet map of a time series consisting of two half cycles of ≈5.5 years (2000 days),

$$f(t) = \sin\left(\frac{2\pi t}{27.5 - 0.00025t}\right), \quad t = 0, 1999 \quad (2)$$

$$f(t) = \sin\left(\frac{2\pi t}{27.5 - 0.00025(t - 2000)}\right), \; t = 2000, 3999 \quad (3)$$

is depicted. This time-series contains a period jump simulating the transit from a foregoing to the following activity cycle.

While at $t = 0$ as well as at $t = 2000$ the observed period should be identical with the intrinsic one according to Eq. (1), there should be a difference of 0.5 days after 5.5 years (as well as 11 years) between them. Thus the wavelet map should show 26.5 days instead of the true 27.0 days after 5.5 years followod by a back jump

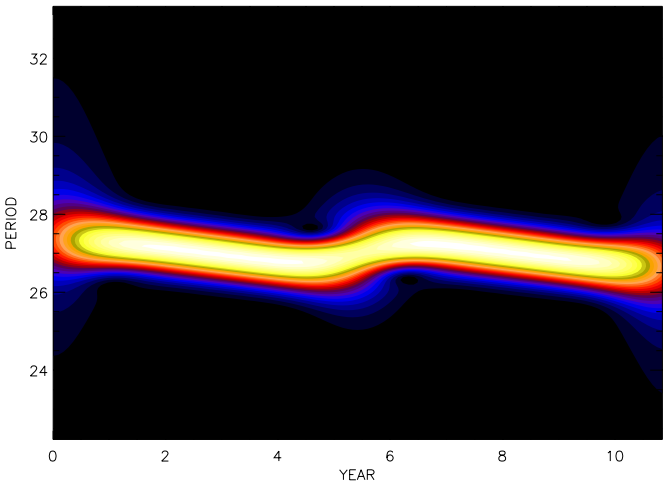

Fig. 4. Wavelet map of simulated rotational modulation with continous period change between 27.5 and 27.0 days over 5.5 years followed by a back-jump to 27.5 days.

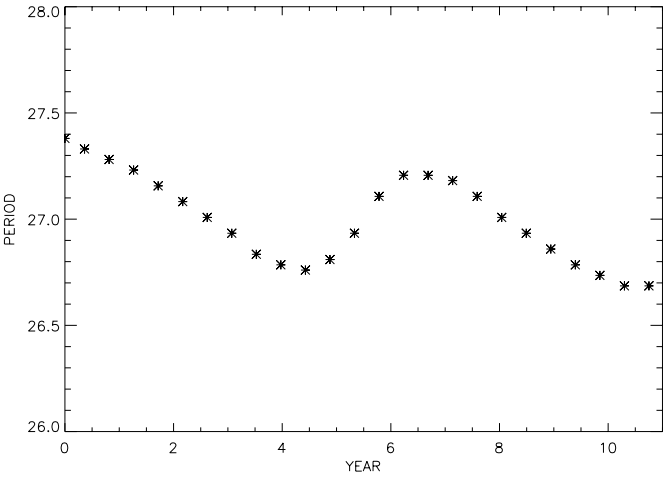

Fig. 5. Run of the maximum power curve of Fig. 4 (butterfly diagram).

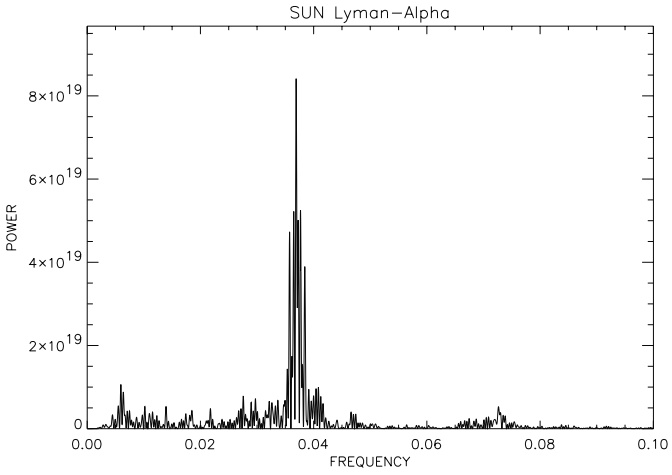

Fig. 6. Fourier spectrum of the Lyman-α time-series.

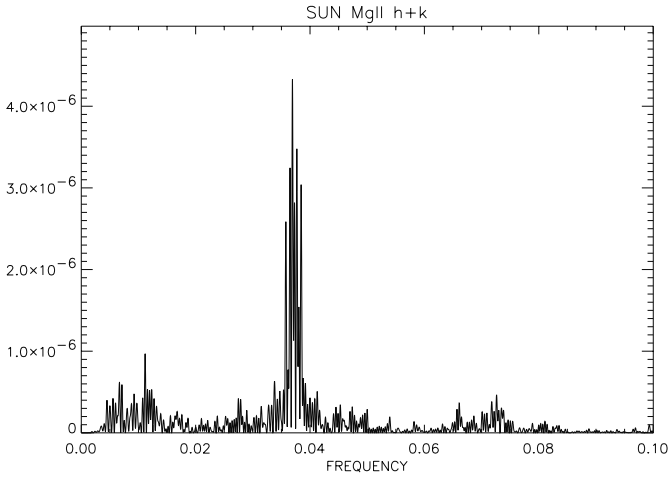

Fig. 7. Fourier spectrum of the MgII h+k time-series.

to 27.5 days. But this is not the case as Figs. 4 and 5 show. Indeed there is an amplitude visible which corresponds to the intrinsic value of 0.5 days. Furthermore, the observed period starts with a lower value as expected and the whole curve is shifted down. The reason is limited time resolution which i) damps each jump in period change and, ii) shifts the median of the wavelet at the beginning to a later time and at the end of the time-series to an earlier time. The balance of these two effects, i.e., period shift and limited time resolution yield the behaviour of Figs. 4 and 5. Accordingly, both effects should be kept in mind and should be minimized by choosing an optimum resolution when analysing stellar butterfly diagrams.

3.3. Discussion

The wavelet maps of the Lyman α and the MgII h+k data are shown in Figs. 8 and 9 where the rotation period is depicted over the year. Both figures look quite similar where maximum power is evident at a costant period of 26.9–27.0 days between 1991 and 1994 followed by splitting in two periods reaching 26.0 and 27.8 days in 1995. Note that the median between them remains constant at 26.9–27.0 days.

Although the wavelet transform power decreases rapidly in both branches during the end of solar cycle 22 there is a jump clearly visible in the beginning of cycle 23. (Because of the limited time resolution the beginning of this jump must appear before the onset of the new cycle.) The direction of the jump is what we expect from solar differential rotation. However, the splitting into two periods continues also during cycle 23 until the end of the time-series analysed is reached in 1999.

While the direction of period change starting in 1996 can be understood easily the period splitting remains as an open question and hampers a quantitative analysis of differential rotation amplitude hidden in the data. Presumably it is a further artefact resulting from zero phase modulation. As Szatmári et al. (1994) have shown, splitting in two modes is typical for phase jumps while cyclic modulation of any parameter tends to lead to splitting into three components. Figure 13 (middle picture)

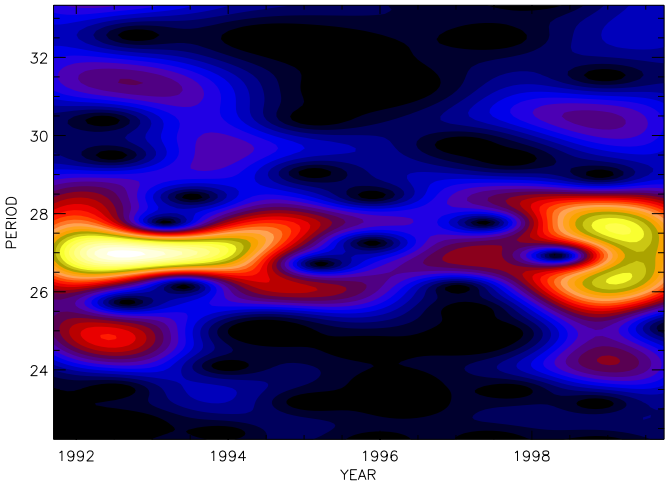

Fig. 8. Wavelet map of the Lyman α data.

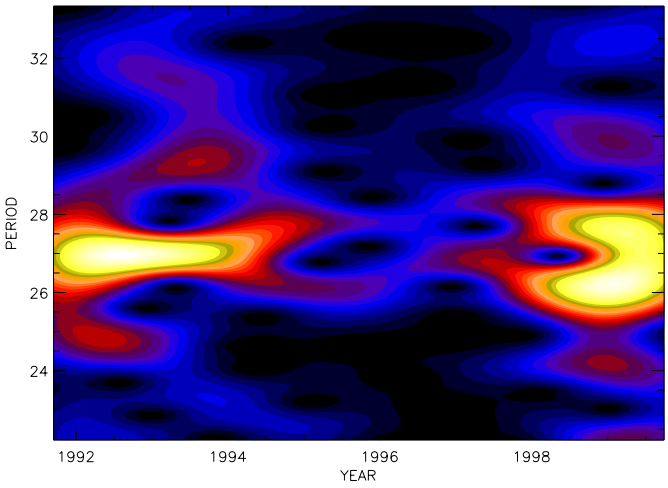

Fig. 9. Wavelet map of the MgII h+k data.

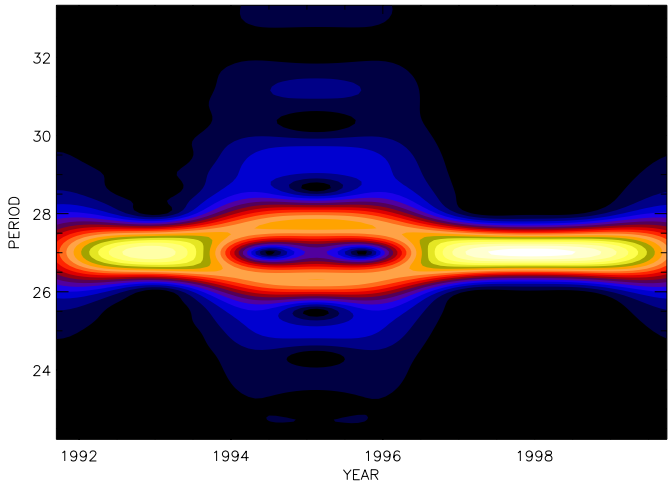

Fig. 10. Wavelet map of an artificial time-series: $y_i = \sin(i * 2\pi/\mathrm{P})$, i = 1,...1000; $y_i = \sin(i * 2\pi/\mathrm{P} + \pi)$, i = 1001,...1500; $y_i = \sin(i * 2\pi/\mathrm{P})$, i = 1501,...3000. Start time is set to 1991.7.

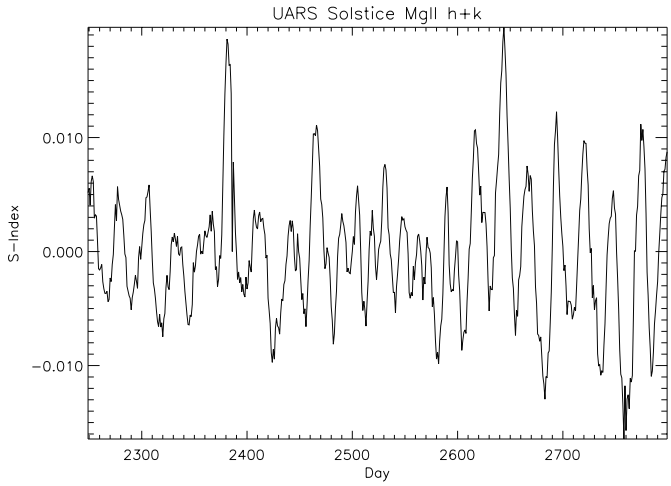

Fig. 11. Detail of the MgII h+k time-series observed in 1998.

of their paper suggests a wavelet map similar to those found here. To test this in more detail an artificial time series was created and analysed. It contains the same basic values as the solar data but included a phase jump of 180° at time 1994.4 followed by a back jump to 0° at time 1995.8. Figure 10 shows the result. Indeed a splitting into two components of equal strengths is visible. Further experiments have shown that the width of splitting does not depend on the jump value but the relative power of the two branches: a 90° jump enhances the power in the lower period band, a 270° jump causes just the oppsite. Note further that the splitting appears and vanishes before and after the actual jumps. This behaviour results from the finite time resolution. It is also responsible for the long lasting of splitting of two years (Fig. 10). A higher time-resolution would offer a region between the phase jumps where splitting would disappear.

The long-lasting splitting seen in Figs. 8 and 9 indicates a sequence of phase jumps. Four consecutive holes between the two branches of enhanced power are visible reflecting most probably four jumps. Increasing the time-resolution in the wavelet map by lowering the value of the parameter a yields a more accurate estimate of the time when a jump appeared. Figure 11 shows a detail of Fig. 3 centered on the time of the last jump which appeared in 1998. This figure shows that the period of modulation is much longer at the beginning and the end compared to the middle of Fig. 11. A quantitative analysis yields a period in the middle range which is the *half* the solar rotation period. This suggests that it is the result of two regions of enhanced net emission in MgII h+k which are located on opposite solar longitudes. At the beginning and also at the end the period of modulation corresponds to *one* solar rotation and therefore must result from a net concentration of emissivity on one longitude. The modulation at the end is phase shifted to the beginning, too. Altogether, this proves that active region decay on one side of the Sun and growth on the opposite side took place simultaneously and result finally in a change of the phase of rotational modulation of 180°.

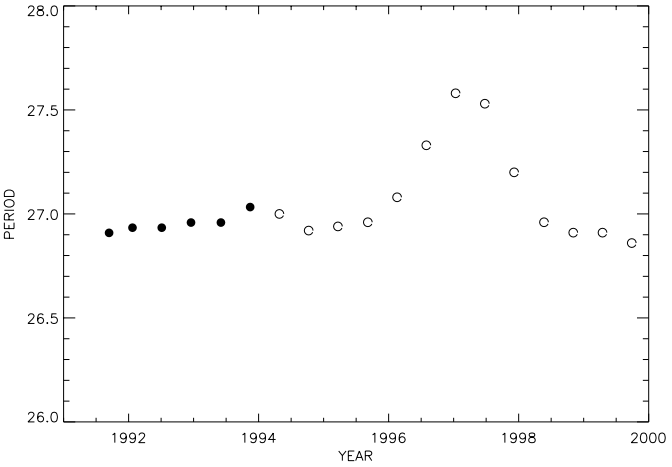

Fig. 12. Butterfly diagram derived from the wavelet map. Open circles: median of the two branches.

The conclusion is that in case of phase jumps the true rotation period must be taken as the median of the two branches (Fig. 12). It follows from Fig. 12 that no change of the rotation period is visible in the data between 1992 and the end of cycle 22. It was stable on 26.9–27.0 days. In 1997 the period of modulation changed to 27.6 days which I interprete as the result of the net emission shifting to regions at higher solar latitude as the consequence of the onset of solar cycle 23. During the following time the period changed continously to lower values until the end of the time-series in late 1999 where a rotation period of 26.8 days was observed.

Deriving solar differential rotation from extrapolating their trend up to the end of cycle 23 will be somewhat speculative. However, the appearence of period constancy at the end of cycle 22 and reaching almost the same value in late 1999 makes a similar behaviour for cycle 23 conceivable. The amplitude of 0.8 days is lower than the finding of Paper I where CaII K line emission data of the Sun were analysed. The amplitude there was a factor two higher which seems to be a bit too high when compared to Fig. 10 in the paper by Gray & Baliunas (1997). Another point is that both estimates differ not only in amplitude but also in their mean values by 0.5 days. It is known that estimates of differential rotation are strongly dependent of the tracer used (cf., Cox 2000). For example, the equatorial rotation rates of plages (Howard 1990) and supergranulation (Duvall 1980; Snodgrass & Ulrich 1990) differ by one day. While the mean CaII K period of Paper I satisfactorily agreed with plages only, the period derived here from tracers in the ultraviolet is somewhat shifted in the direction of supergranulation.

4. Conclusions

The Solstice UARS data where the Sun is observed as a star in the ultraviolet show strong and clear rotational modulation as well as variations with the solar cycle from the end of cycle 22 until the beginning of cycle 23. Accordingly the Solstice data should be well suited for the detection of solar surface differential rotation. Differential rotation is visible both in a period jump at the time when cycle 23 has started and in a following trend to shorter periods. However, differential rotation is not visible in the foregoing part of cycle 22. Intervals of constancy were also found in Paper I. It appears doubtful whether time-series not covering a complete activity cycle can exhibit the correct result.

The wavelet map shows continuous period splitting into two periods of equal power and also equal spacing around the true period over years and even continuing over the transition from solar cycle 22 to cycle 23. It is shown that this behaviour is explained by a sequence of four jumps of 180° in phase of rotational modulation caused by active region growth and decay (ARGD). At least in one case ARGD could be studied in detail. It demonstrates that ARGD plays an important role and hampers strongly each kind of analysis. However, wavelet analysis has the great advantage of clarity where the complex behaviour is visible at first sight.

Acknowledgements. I thank Prof. Dr. G. Rüdiger (Potsdam) who has suggested this work. I am also indepted to an anonymous referee who suggested a set of improvements.

References

Baliunas, S. L., Horne, J. H., Porter, A., et al. 1985, ApJ, 294, 310
Chandra, S., Lean, J. L., White, O. R., et al. 1995, Geoph. Res. Lett., 22, 2481
Cox, A. N. (ed.) 2000, Allen's Astrophysical Quantities (AIP Press New York)
Donahue, R. A., & Keil, S. L. 1995, Solar Phys., 159, 52
Donahue, R. A., Saar, S. H., & Baliunas, S. L. 1996, ApJ, 466, 384
Duvall, Jr. T. L. 1980, Solar Phys., 66, 213
Foukal, P. 1998, ApJ, 500, 958
Howard, R. F. 1990, Solar Phys., 126, 299
Gray, D. F., & Baliunas, S. L. 1997, ApJ, 475, 303
Hempelmann, A., & Donahue, R. A. 1997, A&A, 322, 835
Kitchatinov, L. L., & Rüdiger, G. 1995, A&A, 299, 446
Kitchatinov, L. L., & Rüdiger, G. 1999, A&A, 344, 911
Knapp, B. G. 2000, `http://lasp.colorado.edu/solstice/solsticehome.html`, `solstice lya2.dat` and `solstice mgii2.dat`
Rottman, G. J., Woods, T. N., & Sparn, T. P. 1993, J. Geophys. Res., 98, 10667
Rottman, G. J. 1999, J. Atmospheric Solar-Terr. Phys., 61, 37
Skumanich, A., Lean, J. L., Livingston, W. C., & White, O. R. 1984, ApJ, 282, 776
Snodgrass, H. B., & Ulrich, R. 1990, ApJ, 351, 309
Szatmáry, K., Vinkó, J., & Gál, J. 1994, A&AS, 108, 377
Woods, T. N., Rottman, G. J., & Ucker, G. J. 1993, J. Geophys. Res., 98, 10679
Woods, T. N., Prinz, D. K., Rottman, G. J., et al. 1996, J. Geophys. Res., 101, 9541
Woods, T. N., Tobiska, W. K., Rottman, G. J., & Worden J. R. 2000, J. Geophys. Res., 105, 27195
Worden, J. R., White, O. R., & Woods, T. N. 1998, ApJ, 496, 998